



# Water Resources Research®



## RESEARCH ARTICLE

10.1029/2025WR039989

# Pore-Scale Study of Non-Clogging Accumulation Effects on Microgel Particle Transport and Multiphase Displacements in Porous Media

Xukang Lu<sup>1</sup>, Qiangqiang Li<sup>1</sup>, Jiajun Chen<sup>2</sup>, Tianjiang Wu<sup>2</sup>, Wenhai Lei<sup>3</sup> , and Moran Wang<sup>1</sup> 

<sup>1</sup>Department of Engineering Mechanics, Tsinghua University, Beijing, China, <sup>2</sup>Oil & Gas Technology Research Institute, Changqing Oilfield Company, Xi'an, China, <sup>3</sup>Department of Engineering Mechanics, KTH Royal Institute of Technology, Stockholm, Sweden

### Key Points:

- An improved two-fluid model based on multiphase lattice Boltzmann method is applied to model particle-water-nonaqueous phase flow
- Particle lagging driven by pore-to-throat variations under concentration-sensitive viscosity reshapes particle transport in porous media
- Significant flow diversion can be achieved by accumulation of microgel particles during multiphase displacement

### Supporting Information:

Supporting Information may be found in the online version of this article.

### Correspondence to:

M. Wang,  
mrwang@tsinghua.edu.cn

### Citation:

Lu, X., Li, Q., Chen, J., Wu, T., Lei, W., & Wang, M. (2025). Pore-scale study of non-clogging accumulation effects on microgel particle transport and multiphase displacements in porous media. *Water Resources Research*, 61, e2025WR039989. <https://doi.org/10.1029/2025WR039989>

Received 16 JAN 2025

Accepted 27 MAY 2025

### Author Contributions:

**Conceptualization:** Moran Wang  
**Data curation:** Jiajun Chen, Tianjiang Wu  
**Investigation:** Xukang Lu  
**Methodology:** Xukang Lu, Qiangqiang Li  
**Project administration:** Moran Wang  
**Resources:** Tianjiang Wu  
**Software:** Wenhai Lei  
**Supervision:** Moran Wang  
**Writing – original draft:** Xukang Lu  
**Writing – review & editing:** Wenhai Lei, Moran Wang

© 2025 The Author(s).

This is an open access article under the terms of the [Creative Commons Attribution-NonCommercial License](https://creativecommons.org/licenses/by/4.0/), which permits use, distribution and reproduction in any medium, provided the original work is properly cited and is not used for commercial purposes.

**Abstract** Particle transport in subsurface porous media under multiphase flow conditions is widely concerned in many practical applications. Previous studies have focused on retention behaviors and interfacial effects, ignoring the unique role of pronounced rheological effect under dilute conditions. Here, we investigate how accumulation effect reshapes microgel particle transport and immiscible displacement process driven by concentration-sensitive viscosity. As a foundation, a mixture-rheology two-fluid model is developed and combined with color-gradient lattice Boltzmann method for modeling complex particulate multiphase flow. The consistency between simulation results and microfluidic experiments confirms the validity of our model in capturing accumulation phenomena. Results in heterogeneous dual-permeability structures reveal the two-way coupling between particle accumulation and interfacial evolution. Particle accumulation can be enhanced at higher injection concentrations and larger particle sizes, leading to the formation of filter-cake-like structures despite the absence of clogging effects. Capillary resistance further weakens the driving force for particle migration, intensifying local accumulation compared to suspension flow. The non-uniform concentration distribution contributes to flow rate reallocation via diversion effects, producing variable displacement patterns under varying conditions. Results in disordered media exhibit a similar trend as in the dual-permeability model but with more significant accumulation. The dramatic reduction in nonaqueous phase saturation by sweeping efficiency improvement indicates the promising application potential of such accumulation. Our findings deepen the understandings of particle transport in porous media with implications for manipulation of immiscible displacement.

## 1. Introduction

Particle transport under multiphase flow conditions is of vital importance in many subsurface scenarios, including but not limited to in situ degradation of nonaqueous phase liquid (NAPL) contaminants via engineered nanoparticles (O'Carroll et al., 2013; Pak et al., 2020), pathogen migration in unsaturated vadose zones (Sim & Chrysikopoulos, 2000; Y. Yu et al., 2021), and enhanced removal of NAPL by particle suspensions (Du et al., 2021; Lei et al., 2023; Zhang et al., 2016). Extensive efforts have been made to understand the relationship between particle transport behaviors and multiphase flow patterns. On the one hand, particle retention induced by clogging effects such as size exclusion (Gerber et al., 2018), bridging (Yin et al., 2024), deposition (Bizmark et al., 2020), and aggregation (Katzourakis & Chrysikopoulos, 2021), can dramatically decrease the local permeability and divert the displacing fluid into other regions (Bai et al., 2007; Xie et al., 2021). On the other hand, particles with surface activity can adsorb onto the interfaces, which has been utilized to reduce interfacial tension and mobilize organic contaminants (Roy & Dzombak, 1997; Xu et al., 2015).

Aside from retention behaviors and interfacial effects, fluid rheology changes induced by particles provide an alternative way for multiphase flow control in porous media. In contrast to the weak viscosity effect of hard-sphere particles in dilute conditions (Batchelor, 1977; Guazzelli & Pouliquen, 2018), microgel particles have been found to significantly change suspension viscosity even at dilute concentrations attributed to the polymeric network structure (Larson & Desai, 2015; H. Wang et al., 2018; Lu & Wang, 2023). Microfluidic experiments have shown that increased viscosity of microgel particle suspensions promotes more uniform displacement patterns in heterogeneous porous media, which can be well modeled using the advection-diffusion equation (ADE) in analogy to polymer solutions (Lei et al., 2022). However, when the injection concentration is further increased, significant particle accumulation is observed despite the small particle-to-throat size ratio and

negligible adsorption effect. Core-scale studies (Endo Kokubun et al., 2019; Spildo et al., 2009) have also reported similar phenomena, which cannot be simply explained by rheological effects.

Particle accumulation in the absence of clogging effects is commonly ignored in subsurface flow conditions attributed to the low characteristic speed and negligible inertial effect (Koch & Hill, 2001; Wood, 2007). However, the complex and continuous geometry changes in disordered porous media can naturally induce particle lagging. When particle concentration and rheological property are strongly correlated, the interplay between interphase drag and viscosity changes can reshape particle transport patterns, which may have important implications for controlling interfacial evolution during immiscible displacement.

Numerical modeling provides a powerful tool for insights into the underlying mechanism. Eulerian–Lagrangian methods, such as immersed boundary method (IBM) and discrete element method (DEM), have been developed for accurate simulation of particulate flow in porous media (Chu et al., 2010; Ladd, 1994; Trofa et al., 2021; Zhu et al., 2007). The pressure fluctuations (Lei et al., 2019; Zhou et al., 2017) and diversion effects (Elrahmani et al., 2023; Su et al., 2019) induced by various clogging behaviors with non-uniform distribution of particles have been extensively discussed based on simulation results. There are also pore-network modeling studies that ignore collision effects while introduce criteria for different retention events (Lin et al., 2021; H. Yang & Balhoff, 2017). Eulerian–Eulerian methods, which treat suspended particles as a continuum phase, can greatly improve the computational efficiency by neglecting microscopic details (Drew, 1983). The two-fluid model (TFM) is a representative Eulerian–Eulerian method suitable for capturing particle–fluid and interparticle interactions, which has been widely applied in simulations of fluidized bed (Gidaspow, 1994; van der Hoef et al., 2008), dispersed gas–liquid systems (He et al., 2007; T. Wang & Wang, 2005), and blood flow (Massoudi et al., 2012; Wu et al., 2015). Volume-averaged equations for both the particle phase and fluid phase are solved, where the particle–fluid interaction is characterized by the drag force term (Wen & Yu, 1966). However, the artificial and sophisticated construction of viscosity models for the particle phase (Ding & Gidaspow, 1990; Grad, 1949; Shuai et al., 2012) brings uncertainty to the validity of numerical modeling, especially when dealing with complex particle systems. Furthermore, coupling of the TFM with immiscible displacement simulation has not been reported yet, which involves simultaneous three-phase flow.

In the present work, we comprehensively reveal non-clogging accumulation effect on microgel particle transport and immiscible displacement in porous media. An improved two-fluid model based on multiphase lattice Boltzmann method is applied to efficiently solve particulate multiphase flow. The accuracy and validity of our model are verified by theoretical benchmarks and comparison with previous microfluidic experiments, especially in capturing lagging and accumulation behaviors of microgel particles under multiphase conditions. Simulations of suspension displacement processes in the dual-permeability model are conducted under various injection conditions. The impacts of flow and structure characteristics, particle properties, and immiscible interfaces on accumulation states are analyzed in detail, which will influence interfacial evolution and alter displacement patterns. The potential applications of microgel particle suspensions in preferential flow control and displacement enhancement is further evaluated in complex disordered geometry. Our results offer valuable insights into particle transport mechanisms in subsurface environments, providing an effective approach for flow control in porous media.

## 2. Methods and Validations

### 2.1. Mixture-Rheology Two-Fluid Model (mrTFM)

The two-fluid model (TFM) is adopted in this work considering the computational cost for the simulation of transport and displacement processes involving large amounts of particles. Based on continuum-mechanical descriptions, the volume-averaged governing equations for the particle and fluid phases are given as

$$\frac{\partial(\phi_f \rho_f)}{\partial t} + \nabla \cdot (\phi_f \rho_f \mathbf{u}_f) = 0, \quad (1)$$

$$\frac{\partial(\phi_p \rho_p)}{\partial t} + \nabla \cdot (\phi_p \rho_p \mathbf{u}_p) = 0, \quad (2)$$

$$\frac{\partial(\phi_f \rho_f \mathbf{u}_f)}{\partial t} + \nabla \cdot (\phi_f \rho_f \mathbf{u}_f \mathbf{u}_f) = -\phi_f \nabla P + \nabla \cdot (\phi_f \mathbf{\Gamma}_f) - \beta(\mathbf{u}_f - \mathbf{u}_p) + \mathbf{F}_{\text{ext},f}, \quad (3)$$

$$\frac{\partial(\phi_p \rho_p \mathbf{u}_p)}{\partial t} + \nabla \cdot (\phi_p \rho_p \mathbf{u}_p \mathbf{u}_p) = -\phi_p \nabla P + \nabla \cdot (\phi_p \mathbf{\Gamma}_p) + \beta(\mathbf{u}_f - \mathbf{u}_p) + \mathbf{F}_{\text{ext},p}, \quad (4)$$

where the subscript  $f$  and  $p$  indicate the fluid phase and particle phase, and  $\phi$ ,  $\rho$ ,  $P$ ,  $\mathbf{u}$ ,  $\mathbf{F}_{\text{ext}}$  are the volume fraction, phase density, pressure, velocity, and external forces, respectively.  $\mathbf{\Gamma}_i = \mu_i(\nabla \mathbf{u}_i + (\nabla \mathbf{u}_i)^T)$  is the shear stress tensor, where  $\mu_i$  is the dynamic viscosity.

Fluid-particle interactions are reflected by the drag force term  $\mathbf{F}_d = \beta(\mathbf{u}_f - \mathbf{u}_p)$  induced by velocity difference, where  $\beta$  is the drag force coefficient that can be described by the Wen-Yu model as (Wen & Yu, 1966)

$$\beta = \frac{3}{4} C_d \frac{\rho_f \phi_f \phi_p |\mathbf{u}_f - \mathbf{u}_p|}{d_p} \phi_f^{-2.65}, \quad (5)$$

where  $d_p$  is the particle diameter,  $C_d$  is the dimensionless drag coefficient,  $C_d = 24(1 + 0.15Re_d^{0.687})/Re_d$  for  $Re_d < 10^3$  and  $Re_d = \rho_f \phi_f d_p |\mathbf{u}_f - \mathbf{u}_p| / \mu_f$  is the characteristic Reynolds number for drag force calculation.

For the suspension phase as a whole, the governing equations can be expressed as

$$\frac{\partial \rho_s}{\partial t} + \nabla \cdot (\rho_s \mathbf{u}_s) = 0, \quad (6)$$

$$\frac{\partial(\rho_s \mathbf{u}_s)}{\partial t} + \nabla \cdot (\rho_s \mathbf{u}_s \mathbf{u}_s) = -\nabla P + \nabla \cdot \mathbf{\Gamma}_s + \mathbf{F}_{\text{ext}}. \quad (7)$$

In the conventional TFM, governing equations for the particle and fluid phases (Equations 1–4) are solved simultaneously. As mentioned in the introduction part, an important issue in applying the TFM is to formulate the stress tensor in the viscous resistance term of the particle phase. Regarding complex particle systems such as blood and microgel particle suspensions, it is challenging to build rheology models directly from microscopic interparticle interactions. Additional empirical models or parameters are required to incorporate the concentration-dependent non-Newtonian feature of suspensions into the particle phase viscosity (Wu et al., 2015), which bring about uncertainty and inaccuracy in transport simulations.

Therefore, we propose the mixture-rheology two-fluid model (mrTFM) by considering the mixture (suspension) phase and the fluid phase without involving the particle phase viscosity. The viscosity of the mixture phase is based on the apparent suspension property with a clear physical basis, which can be conveniently characterized via experiments and directly applied in simulations. Information about microscopic interactions is effectively reflected in the apparent rheological property, and particle transport can be solved accurately without introducing any empirical models. Numerical stability can also be improved with a smaller viscosity difference between the simulated two phases. For suspensions with viscosity sensitive to particle concentration (as discussed in this work), the particle phase viscosity must be extremely high if the conventional TFM is adopted, posing significant challenges to numerical stability. Furthermore, coupling two-phase particulate flow with displacement simulations is more feasible, as the suspension phase has been explicitly solved in the first step.

For the sake of simplicity and without loss of generality, the particle-water-NAPL system will be taken as an example, where particles are suspended in water with immiscible interfaces between water and NAPL. For particle-water two-phase flow, the suspension phase and the fluid phase are solved simultaneously based on the mrTFM, as illustrated in Figure 1a. Information regarding the particle phase (particle volume fraction  $\phi_p$  and particle phase velocity  $\mathbf{u}_p$ ) can be calculated by local mass and momentum conservation, which serves as an input for the drag force calculation. For particle-water-NAPL three-phase flow, the suspension phase and the NAPL with interfaces are solved simultaneously after obtaining the information of particle-water two-phase flow. The particle-water two-phase flow and particle-water-NAPL three-phase flow will be respectively referred to as suspension flow and suspension displacement in the following text.

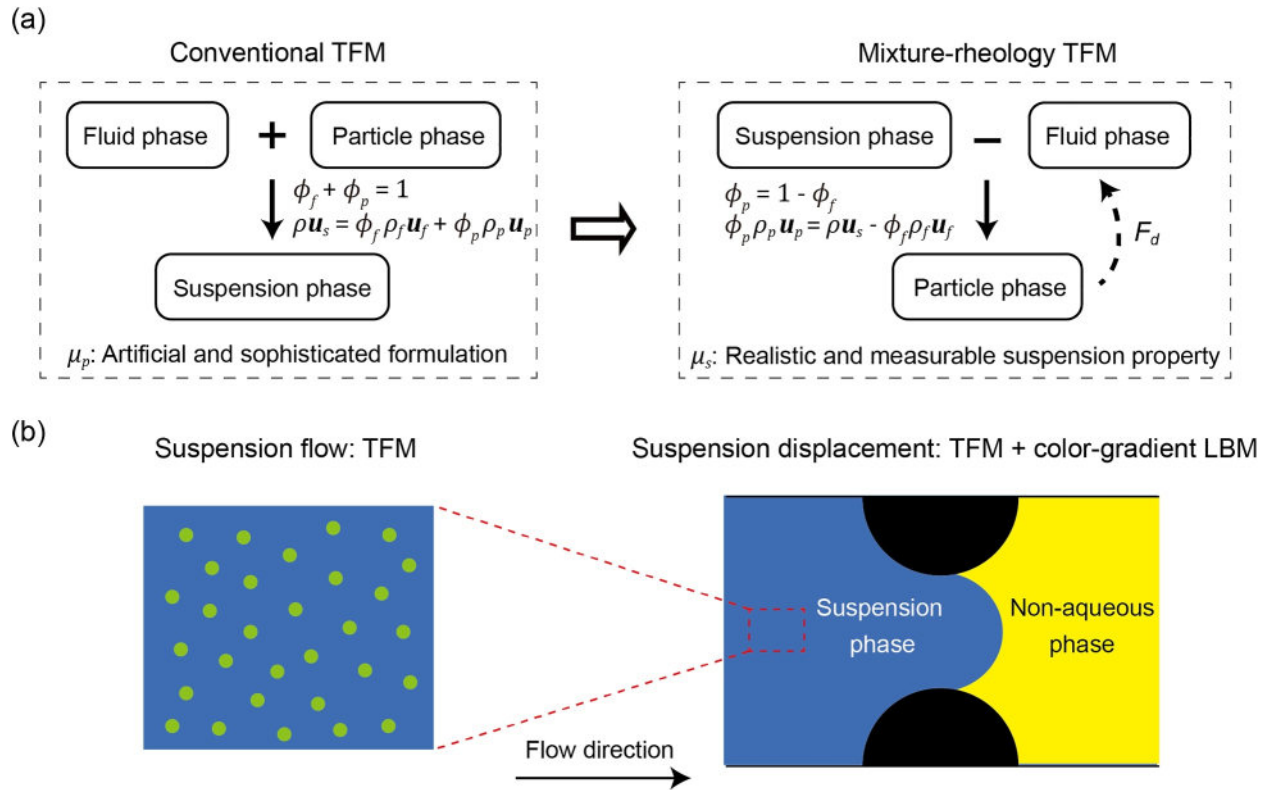


**Figure 1.** (a) Schematic of the difference between conventional TFM and mixture-rheology TFM. (b) Schematic of the three-phase system. The particle-water-NAPL system is taken as an example.

## 2.2. Numerical Method for Particulate Multiphase Flow

The lattice Boltzmann method (LBM) is adopted in this work for solving complex fluid flow in porous media (Chen & Doolen, 1998; Dye et al., 2016; Qin et al., 2023; Xie et al., 2021). The GPU computing based on the CUDA platform is adopted to improve computational efficiency (G. Yang et al., 2023). The initialization, input and output of data are performed on CPU host while the key evolution steps, including collision, recoloring, and streaming, are computed on the GPU device (NVIDIA V100). All simulations are solved in 2D using a standard D2Q9 lattice set.

For suspension flow, evolutions of the suspension phase and the water phase are solved based on the mrTFM. The lattice Boltzmann equation with multiple relaxation times (MRT) can be expressed as

$$f_i(\mathbf{x} + \mathbf{e}_i \Delta t, t + \Delta t) - f_i(\mathbf{x}, t) = -\mathbf{M}^{-1} \mathbf{S}(\mathbf{m}(\mathbf{x}, t) - \mathbf{m}^{\text{eq}}(\mathbf{x}, t)) + \Delta t \mathbf{M}^{-1} \left( \mathbf{I} - \frac{\mathbf{S}}{2} \right) \mathbf{G}, \quad (8)$$

where  $f_i(\mathbf{x}, t)$  is the density distribution function at the space-time position  $(\mathbf{x}, t)$ , moving along the  $i$ th direction by discrete velocities  $\mathbf{e}_i$  (unit vector).  $\mathbf{M}$  is the transformation matrix to the moment space (Lallemand & Luo, 2000),  $\mathbf{m} = \mathbf{M} \mathbf{f}$  is the mapped moment of distribution functions, and  $\mathbf{m}^{\text{eq}} = \mathbf{M} \mathbf{f}^{\text{eq}}$ .  $\mathbf{G} = \mathbf{M} \hat{\mathbf{F}}$  accounts for the forcing term in the moment space, where  $\hat{\mathbf{F}}$  is calculated using Guo's forcing scheme (Guo et al., 2002; Semiao & Silva, 2012).  $\mathbf{I}$  is the unit tensor and  $\mathbf{S}$  is a diagonal matrix composed of relaxation parameters (Z. Yu & Fan, 2010).

The macroscopic variables can be related to  $f_i$  as

$$\rho = \sum_i f_i \cdot \rho \mathbf{u} = \sum_i f_i \mathbf{e}_i + \frac{\Delta t}{2} \mathbf{F}. \quad (9)$$

The body force only needs to be introduced in the evolution equation of the fluid (water) phase for the mrTFM, which includes two key terms

$$\mathbf{F}_f = P\nabla\phi_f - \beta(\mathbf{u}_f - \mathbf{u}_p), \quad (10)$$

where the first term is the correction for pressure gradient considering volume average (T. Wang & Wang, 2005) and the second term is the drag force. The gradient terms involved in the algorithm are calculated employing the isotropic gradient scheme with second-order approximation (Leclaire et al., 2011).

As previously mentioned, the microgel particle suspension is a typical non-Newtonian fluid with shear-dependent viscosity (H. Wang et al., 2018). The shear rate  $\dot{\gamma}$  can be expressed as

$$\dot{\gamma} = (2|\Psi_{\alpha\beta}\Psi_{\alpha\beta}|)^{\frac{1}{2}}, \Psi_{\alpha\beta} = \frac{3}{2\rho\tau c^2} \sum_i f_i^{(1)} e_{i\alpha} e_{i\beta}, \quad (11)$$

where  $\Psi$  is the shear rate tensor,  $\tau$  is the relaxation time,  $c = \Delta x/\Delta t = 1$  is the lattice speed, and  $f_i^{(1)} \approx f_i - f_i^{eq}$  (Xie et al., 2016).

For suspension displacement, evolutions of three phases are solved. The suspension flow is solved following the above procedure, and the color-gradient model is applied to capture the suspension-NAPL interface (Leclaire et al., 2013, 2014). The evolution equation of the color-gradient model is

$$g_i^k(\mathbf{x} + \mathbf{e}_i\Delta t, t + \Delta t) - g_i^k(\mathbf{x}, t) = \Omega_i^{2,k} \left[ -M^{-1}S(\mathbf{m}(\mathbf{x}, t) - \mathbf{m}^{eq}(\mathbf{x}, t)) + \Delta t M^{-1} \left( \mathbf{I} - \frac{\mathbf{S}}{2} \right) \mathbf{G} \right], \quad (12)$$

where  $g_i^k(\mathbf{x}, t)$  is the density distribution function of phase  $k$  and  $\Omega_i^{2,k}$  is the recoloring operator to achieve fluid separation. The macroscopic variables can be expressed as

$$\rho = \sum_k \rho^k, \rho\mathbf{u} = \sum_k \rho^k \mathbf{u}^k, \quad (13)$$

where  $\rho^k$  and  $\mathbf{u}^k$  are calculated from Equation 9.

The continuum-surface-force (CSF) model (Brackbill et al., 1992) is applied to achieve surface tension effect by introducing  $\mathbf{F}_{csf} = \gamma\kappa\nabla\rho^N/2$ , where  $\gamma$  is the surface tension,  $\kappa = -[(\mathbf{I} - \mathbf{n} \otimes \mathbf{n}) \cdot \nabla] \cdot \mathbf{n}$  is the interfacial curvature, and  $\rho^N = (\rho^s - \rho^o)/(\rho^s + \rho^o)$  is the color function ( $s$  for the suspension phase and  $o$  for the NAPL).  $\mathbf{n} = \nabla\rho^N/|\nabla\rho^N|$  is the normal vector of interface, which is corrected based on contact angle restrictions at solid boundaries (Akai et al., 2018; Liu et al., 2015).

The recoloring operator  $\Omega_i^{2,k}$  is introduced after collision steps to achieve phase separation as follows (Latva-Kokko & Rothman, 2005)

$$g_i^{**,k} = \frac{\rho^k}{\rho^s + \rho^o} g_i^{*,k} + \varepsilon \frac{\rho^s \rho^o}{\rho^s + \rho^o} \omega_i \frac{\nabla\rho^N \cdot \mathbf{e}_i}{|\nabla\rho^N|}, \quad (14)$$

where  $g_i^*$  and  $g_i^{**}$  are the post-collision and the pre-streaming distribution functions,  $\omega_i$  is the weight function and  $\varepsilon$  is a tunable parameter controlling the interfacial thickness.

The impenetrable condition at the suspension-NAPL interface for the fluid (water) phase in the mrTFM is realized by another recoloring operator as (Riaud et al., 2014)

$$g_i^f = g_i^f + \varepsilon \frac{\rho^f \rho^o}{\rho^s + \rho^o} \omega_i \frac{\nabla\rho^N \cdot \mathbf{e}_i}{|\nabla\rho^N|}. \quad (15)$$

### 2.3. Model Validations and Discussions

The reliability and accuracy of our lattice Boltzmann method for particulate multiphase flow have been verified by a series of theoretical benchmarks including particle suspension and power-law fluid flow in a straight channel, phase separation test, and interfacial properties of three-phase flow during displacement (see the Text S1 in Supporting Information S1 for details and also our previous work (Li et al., 2024)). More importantly, we compare our simulation results with the anomalous accumulation phenomena reported in previous microfluidic experiments, which validate the capability of present model to capture particle transport and distribution patterns under multiphase and porous flow conditions.

As introduced in Section 2.1, realistic rheological property from experiments can be directly applied based on the mrTFM. The complex concentration-dependent shear-thinning property of microgel particle suspensions has been included in the following expression based on rheological experiments under varying conditions (Li et al., 2024),

$$\mu_s = \begin{cases} (142\phi_p^2 - 0.2\phi_p)\dot{\gamma}^{-0.786} + 0.001, \dot{\gamma} < 10 \text{ s}^{-1} \\ 0.163(142\phi_p^2 - 0.2\phi_p) + 0.001, \dot{\gamma} \geq 10 \text{ s}^{-1} \end{cases}, \quad (16)$$

As shown in Figure 2a, previous displacement experiments applying microgel particle suspensions in a dual-permeability model show dramatic particle accumulation at high injection concentration ( $\phi_p = 3.0$  vol%) (Lei et al., 2022). It should be noted that the minimum throat size is more than 10 times larger than the microgel particle size, basically excluding direct clogging by size exclusion (pore size screening) or bridging in such regular geometry. The micron-sized particles with electrostatic repulsions can hardly adsorb onto the surface (Adamczyk & Weroński, 1999), ruling out deposition-induced accumulation. Deformation effects are also negligible considering the small particle-to-channel size ratio, low characteristic speed and dilute injection concentration. It is worth mentioning that dramatic deformation effects dominated by interparticle interactions can be possible for high-concentration flows of highly deformable particles such as blood cells (Chien, 1987; Wu et al., 2015). However, the microgel particles considered in this work are much less soft (Barns et al., 2017; Lei et al., 2023), and interparticle interactions mainly manifest as interactions between stretched surface polymer chain network under dilute conditions, as discussed previously (H. Wang et al., 2018; Lei et al., 2022). Despite excluding direct clogging, surface deposition, and deformation effects in our model, our simulations applying similar parameters yield consistent accumulation patterns with stepped concentration distribution (Figure 2b).

What is responsible for such dramatic accumulation of microgel particles? As discussed above, since other classical colloidal behaviors are not incorporated in the two-fluid model, the non-uniform concentration distribution can only be induced by particle accumulation under geometric variations in porous media, which is determined by the competition between fluid-particle and interparticle interactions. Starting from the governing equation for the particle phase in the TFM (Equation 4), the fluid-particle interaction is represented by the drag force term  $\beta(\mathbf{u}_f - \mathbf{u}_p)$ , and the interparticle interaction is represented by the viscous resistance term  $\nabla \cdot (\phi_p \Gamma_p)$ , where  $\Gamma_p = \mu_p(\nabla \mathbf{u}_p + (\nabla \mathbf{u}_p)^T)$ . For microgel particle suspensions, the high particle phase viscosity strengthens the viscous resistance term, which needs to be balanced by the drag force term with a velocity difference between the particle and fluid phases. For acceleration process during pore-to-throat geometric variations in porous media, the viscous resistance term will increase due to a decrease in characteristic channel size. Consequently, the velocity difference in the drag force term also needs to be increased, corresponding to particle lagging. Based on the momentum conservation  $\rho_s \mathbf{u}_s = \phi_p \rho_p \mathbf{u}_p + (1 - \phi_p) \rho_f \mathbf{u}_f$ , we can expect an increased particle concentration in response to flow condition variations, triggering local accumulation. The increased particle concentration contributes to strengthened viscous resistance term owing to concentration-sensitive viscosity, which further promotes the accumulation. For hard-sphere suspensions, such accumulation phenomenon is rarely reported since viscosity effect is much weaker in dilute conditions, and the role of viscous resistance term can be ignored.

We further quantify the experimental particle concentration distribution by the brightness of fluorescently labeled microgel particles (see the Text S2 in Supporting Information S1 for details of image processing). As presented in Figures 2d–2g, the fair consistency between simulations and microfluidic experiments demonstrates the applicability of our model for predicting microgel particle transport behaviors. The agreement in particle concentration

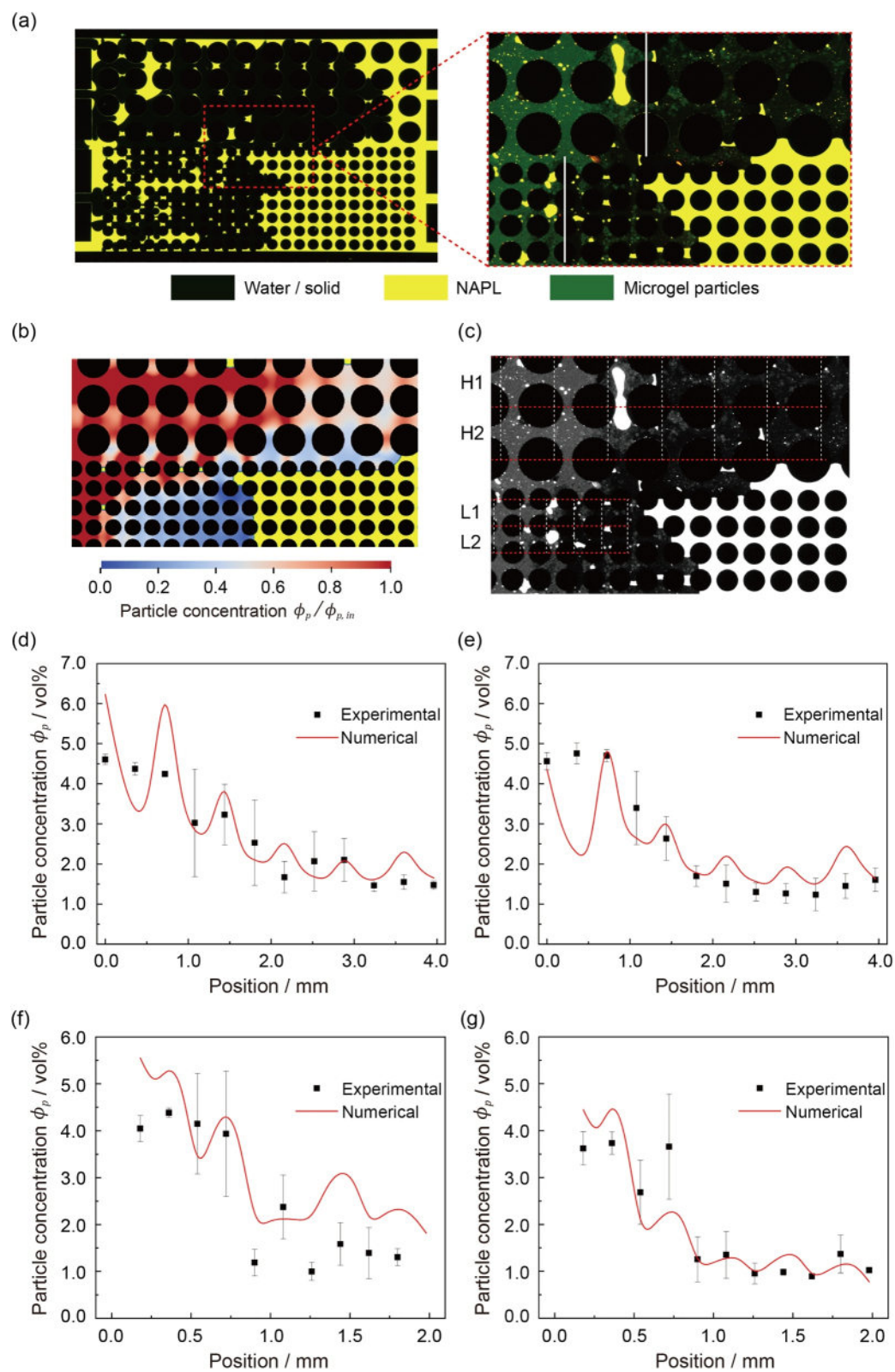


Figure 2.

distribution is quantitatively satisfactory given the impurity of microgel particle suspensions in experiments and the complexity of the multiphase systems.

### 3. Results and Discussion

#### 3.1. Case Setup

We investigate microgel particle transport and flow control mechanisms in the dual-permeability model (Figure 3a) with the same geometry shown in Figure 2. The length and width of the porous region are 8 and 6 mm, respectively. The high-permeability layer (HPL) and low-permeability layer (LPL) yield the same porosity (45%) with a characteristic size ratio of 2:1. To evaluate the impact of complex geometry under more realistic conditions, a disordered medium is generated using the QSGS method (M. Wang et al., 2007) (Figure 3c).

The computational domains are both resolved by  $1620 \times 960$  grids. Grid independence tests have been performed to confirm the reliability of results presented in this work (see Figure S7 in Supporting Information S1). The standard bounce-back scheme is applied to achieve non-slip condition at solid boundaries (including top and bottom wall). The Zou-He boundary (Zou & He, 1997) is applied with constant velocity at the inlet and constant pressure at the outlet. The volume fraction of the particle phase is fixed at the inlet and the zero-gradient Neumann boundary is applied at the outlet to achieve free outflow condition (Lou et al., 2013). For suspension flow, the entire region is filled with water initially and microgel particles are injected at a fixed concentration. For suspension displacement, the porous region is filled with NAPL initially and then the suspension phase (including the particle and water phases) enters from the inlet.

The particle size and injection concentration are varied for comprehensive mechanism analysis:  $d_p = 3 - 6 \mu\text{m}$ ,  $\phi_{p,in} = 1.0 - 5.0 \text{ vol}\%$ . Other physical parameters are set as follows: Inlet velocity  $U_{in} = 0.01 \text{ m/s}$ , density of particle, water and NAPL  $\rho_p = \rho_w = \rho_o = 10^3 \text{ kg/m}^3$ , dynamic viscosity of water and NAPL  $\mu_w = \mu_o = 1 \text{ mPa}\cdot\text{s}$ , contact angle  $\theta = 80^\circ$ , interfacial tension  $\gamma = 6 \text{ mN/m}$ . The dimensionless numbers can be defined based on inlet properties: The particle Stokes number is  $Stk = \rho_p U_{in} d_p^2 / (18 \mu_w W_{in}) = 2 \times 10^{-5} - 8 \times 10^{-5}$ , where  $W_{in}$  is the inlet channel width. For  $Stk \ll 1$ , particles should theoretically follow fluid streamlines with negligible inertial effects (Koch & Hill, 2001), which is contrary to our observations. This indicates that classical description is invalid for reflecting accumulation behaviors reported in this study, as the role of rheological effect representing strong interparticle interactions is ignored. The capillary number for suspension-NAPL displacement is  $Ca = \mu_w U_{in} / \gamma = 1.7 \times 10^{-3}$ .

#### 3.2. Particle Transport and Displacement Control in the Dual-Permeability Model

We first present a series of simulations of two-phase suspension flow without immiscible interfaces to determine impacts of flow, structure, and particle property parameters on particle accumulation patterns. Figure 4a shows evolution of particle concentration distribution when  $d_p = 3 \mu\text{m}$ . At low injection concentration (1.0 vol%), particle front advances rapidly through the HPL. The concentration distribution is relatively uniform after particle breakthrough without accumulation. As injection concentration increases, particle breakthrough is delayed in the HPL with a closer distance between the front in the HPL and LPL (Figure 4b). The delayed breakthrough is attributed to increased flow resistance at higher microgel particle concentrations. Meanwhile, accumulation phenomena are observed owing to the lagging of microgel particles under continuous geometric variations, which have not been captured in previous studies. It is noted that particle accumulation preferentially occurs in regions with lower characteristic permeability, including within the LPL, at the layer interface and edge region, rather

**Figure 2.** Experimental validations. (a) Experimental observation of the stepped particle distribution at 0.5 PV (pore volume) during microfluidic displacement process. The injection concentration is 3.0 vol% and the average particle size is  $5 \mu\text{m}$ . The particles and the oil phase are both fluorescently labeled but with different intensities (Lei et al., 2022). (b) Numerical simulation reproduces the stepped distribution under the same conditions. The flow, structural, and interfacial properties are kept the same as in experiments. Equation 16 is applied as input for the viscosity model. (c) Grayscale experimental image used for processing. As indicated by the dashed boxes, we select four representative regions, divide them into sub-blocks consisting of pore-throat units, and calculate the average particle concentration in each unit. Details of concentration calibration and data processing are provided in the Text S2 in Supporting Information S1. (d–g) Comparison of the particle concentration distribution from experiments and simulations in regions (d) H1, (e) H2, (f) L1, and (g) L2, respectively.

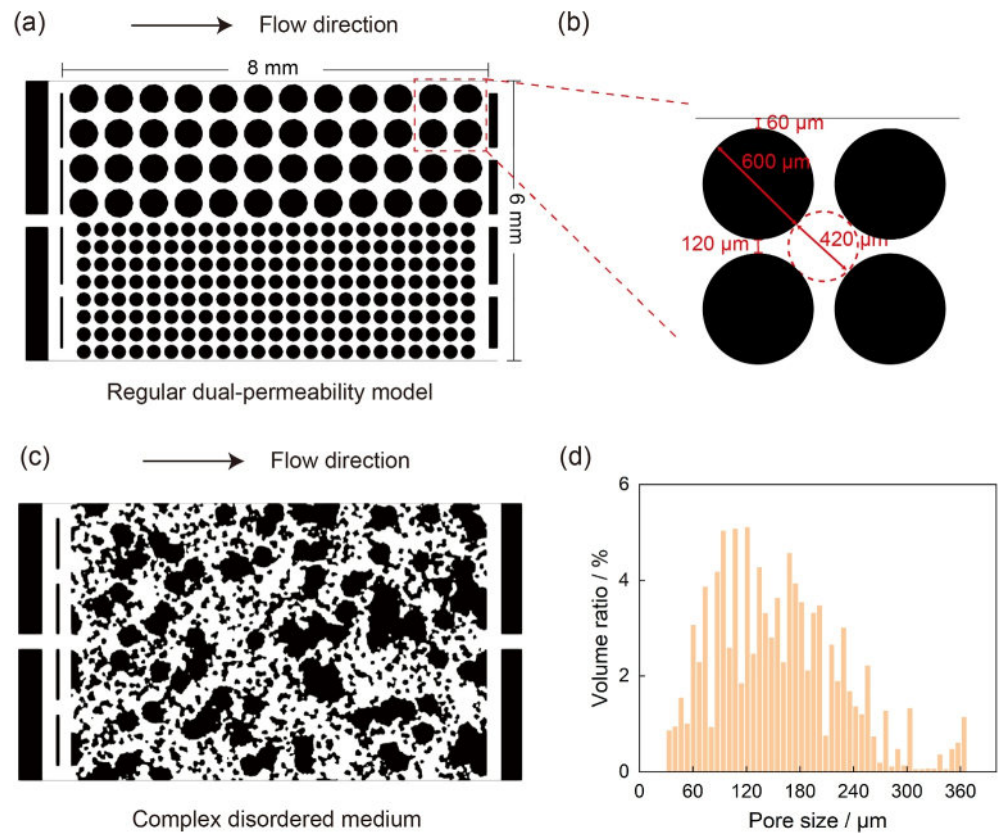


**Figure 3.** Case setup. (a) Dual-permeability model consisting of regular posts. (b) Geometric settings of the cylinders and voids in (a). The characteristic sizes in the low-permeability layer are half of those in the high-permeability layer. (c) Disordered medium with complex geometry. (d) Pore size distribution of (c) characterized by the maximal ball method. The length and width of the porous region are 8 and 6 mm, respectively.

than in the mainstream channels in the HPL. As shown in Figure 4c, accumulation effect is strengthened when  $d_p = 6 \mu\text{m}$ . In the LPL, stronger accumulation results in the filter-cake-like distribution near the inlet with limited in-depth penetration. Such filter-cake-like distribution reflects the dramatic local concentration rise under intensified accumulation, which is essentially different from filter cakes induced by clogging events (Dressaire & Sauret, 2017), where particles are physically stopped. In the HPL, particle accumulation also appears with staggered distribution throughout the layer. The advancing speed of particle front is significantly slowed down in both layers (Figure 4d).

To confirm that the observed accumulation patterns are not limited by the length scale, we have doubled the computational domain, and the results remain consistent (Text S4 in Supporting Information S1). For cases with strengthened accumulation ( $d_p = 6 \mu\text{m}, \phi_p = 3.0 \text{ vol}\%$ ), the filter-cake-like structure in the LPL remains localized near the inlet even though the channel length is extended, indicating separated length scales between the accumulation zone and flow domain. Meanwhile, a more uniform accumulation pattern is observed in the HPL, with in-depth penetration regardless of the domain size.

The above influencing factors on particle accumulation can be well interpreted by the force competition discussed in Section 2.3. The accumulation tendency can be evaluated by the ratio of the drag force  $F_d$  and the viscous resistance force  $F_v$  exerted on the particle phase, given by  $\beta(U_f - U_p)/\nabla \cdot [\phi_p \mu_p (\nabla U_p + (\nabla U_p)^T)]$ , where  $U$  is the velocity along the flow direction. A smaller ratio corresponds to stronger accumulation. Considering the state prior to accumulation without concentration and viscosity gradients, we can obtain  $F_d/F_v \propto (1 - \phi_p)^{-1.65} W^2 / (d_p \mu_p)$ , where  $W$  is the characteristic width and  $\mu_p$  is a function of shear rate and particle concentration. On the one hand, larger particle sizes and higher injection concentrations will hinder

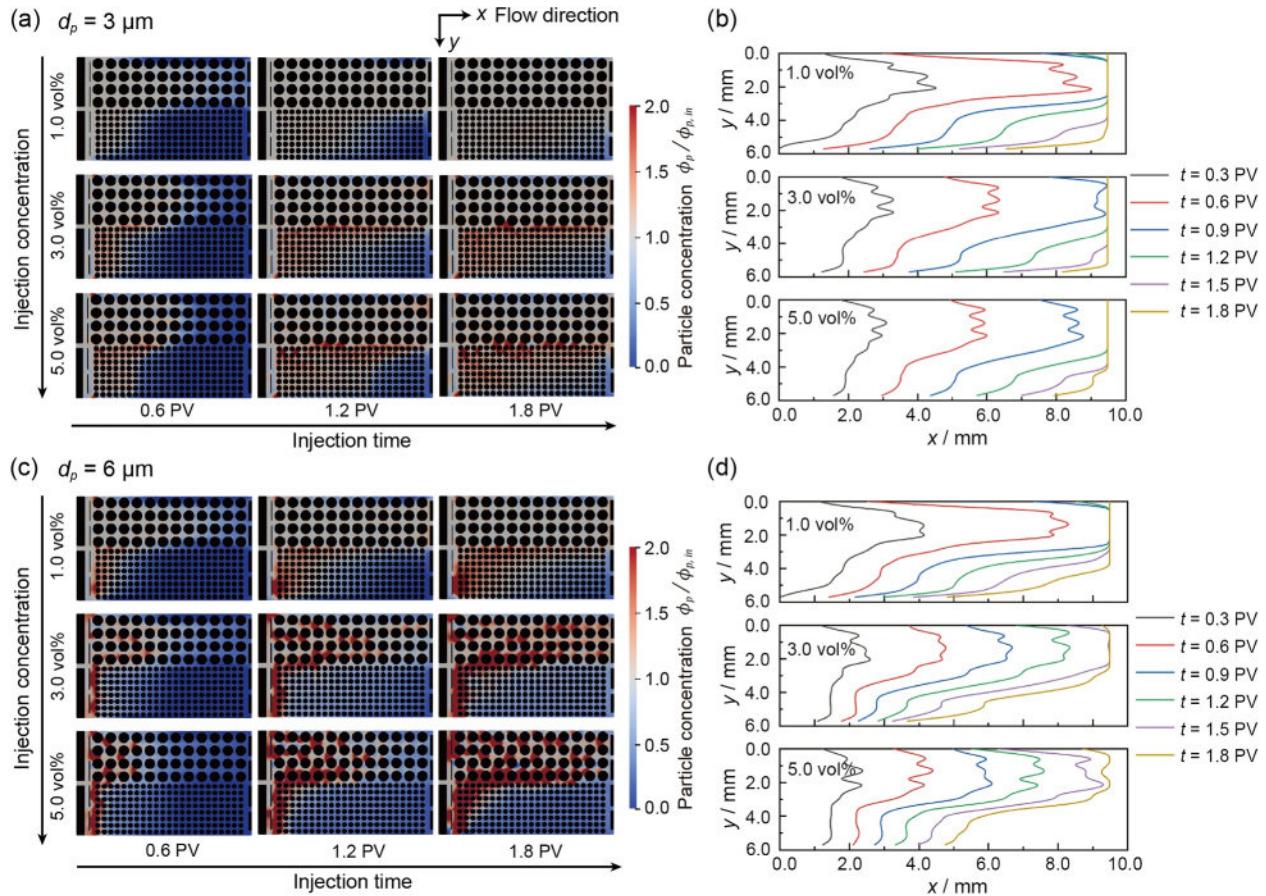


**Figure 4.** Microgel particle transport in the dual-permeability model under suspension flow condition. (a, c) Evolution of particle concentration distribution versus injection time at various injection concentrations. (b, d) Evolution of particle front versus injection time. The corresponding particle sizes are (a, b)  $3 \mu\text{m}$  and (c, d)  $6 \mu\text{m}$ , respectively. The injection time is normalized by the time required to inject one pore volume (PV) of fluid, and the concentration is normalized by the injection concentration  $\phi_{p,in}$ .

particle transport, leading to strengthened accumulation. On the other hand, regions with lower permeability correspond to a lower shear rate and a smaller characteristic size, resulting in preferential accumulation.

As shown in Figure 5, simulations of suspension-NAPL displacement with three-phase flow are further performed in the dual-permeability model. Transport of microgel particles significantly influences evolution of the liquid-liquid interface. At low concentration (1.0 vol%), the suspension phase travels through the HPL rapidly and the NAPL in the LPL remains trapped regardless of the particle size. Such preferential flow feature is induced by the permeability difference between layers, consistent with previous experimental observations (Lei et al., 2022). The viscosity effect (Equation 16) and particle accumulation are relatively weak under low injection concentration, yielding a limited impact on displacement enhancement. At a smaller particle size ( $d_p = 3 \mu\text{m}$ ), the displacement performance is progressively improved when increasing concentration from 1.0 to 5.0 vol%. The suspension phase enters the LPL with more synchronized advances in the two layers. At a larger particle size ( $d_p = 6 \mu\text{m}$ ), similar trend is observed while the difference between 3.0 and 5.0 vol% becomes minor.

Statistics of suspension phase saturation provide quantitative information on concentration and size effects. A monotonic concentration effect on preferential flow control is observed when  $d_p = 3 \mu\text{m}$  with smaller saturation difference between layers (Figure 6a), whereas saturation curves at 3.0 and 5.0 vol% are nearly overlapped when  $d_p = 6 \mu\text{m}$  (Figure 6b). Correspondingly, higher ultimate displacement efficiency is achieved at a smaller size when concentration is high (Figure 6d).

The non-trivial dependence of displacement performance on particle size and concentration essentially reflects the role of particle accumulation patterns. As presented in Figures 7a and 7b, local accumulation is enhanced in

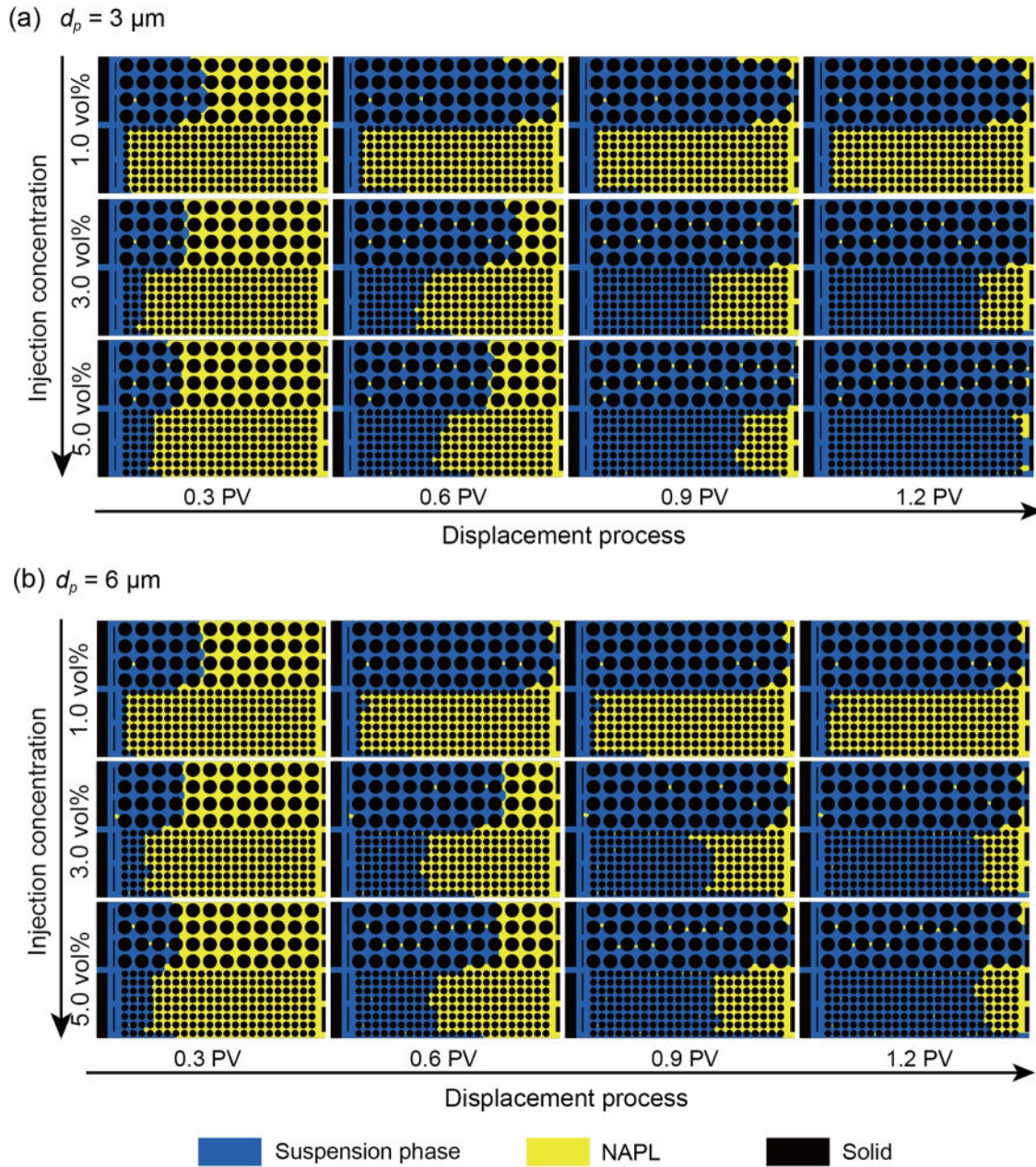


**Figure 5.** Displacement processes in the dual-permeability model. The displacing fluids are microgel particle suspensions at various sizes and injection concentrations.

the presence of immiscible interfaces, as additional capillary resistance is introduced. A filter-cake-like distribution has been formed in the LPL at a smaller particle size ( $d_p = 3 \mu\text{m}$ ), similar to the suspension flow condition at a larger particle size (Figure 4c). The low-concentration region between the particle and interfacial fronts in the LPL drives lateral flow from the HPL to LPL, promoting recovery of residual NAPL. When particle size is increased ( $d_p = 6 \mu\text{m}$ ), filter-cake-like structures form in both layers and a low-concentration region is also created downstream in the HPL. Displacement enhancement is limited by the partial reversal flow from the LPL to HPL (Figure 7c). Therefore, an intermediate accumulation state is more favorable for preferential flow control via moderate diversion effects. As shown in Figure 7d, the coupling of interfacial evolution and particle accumulation induces flow rate interchange between layers with fluctuated net lateral flow rate at large particle size and high injection concentration.

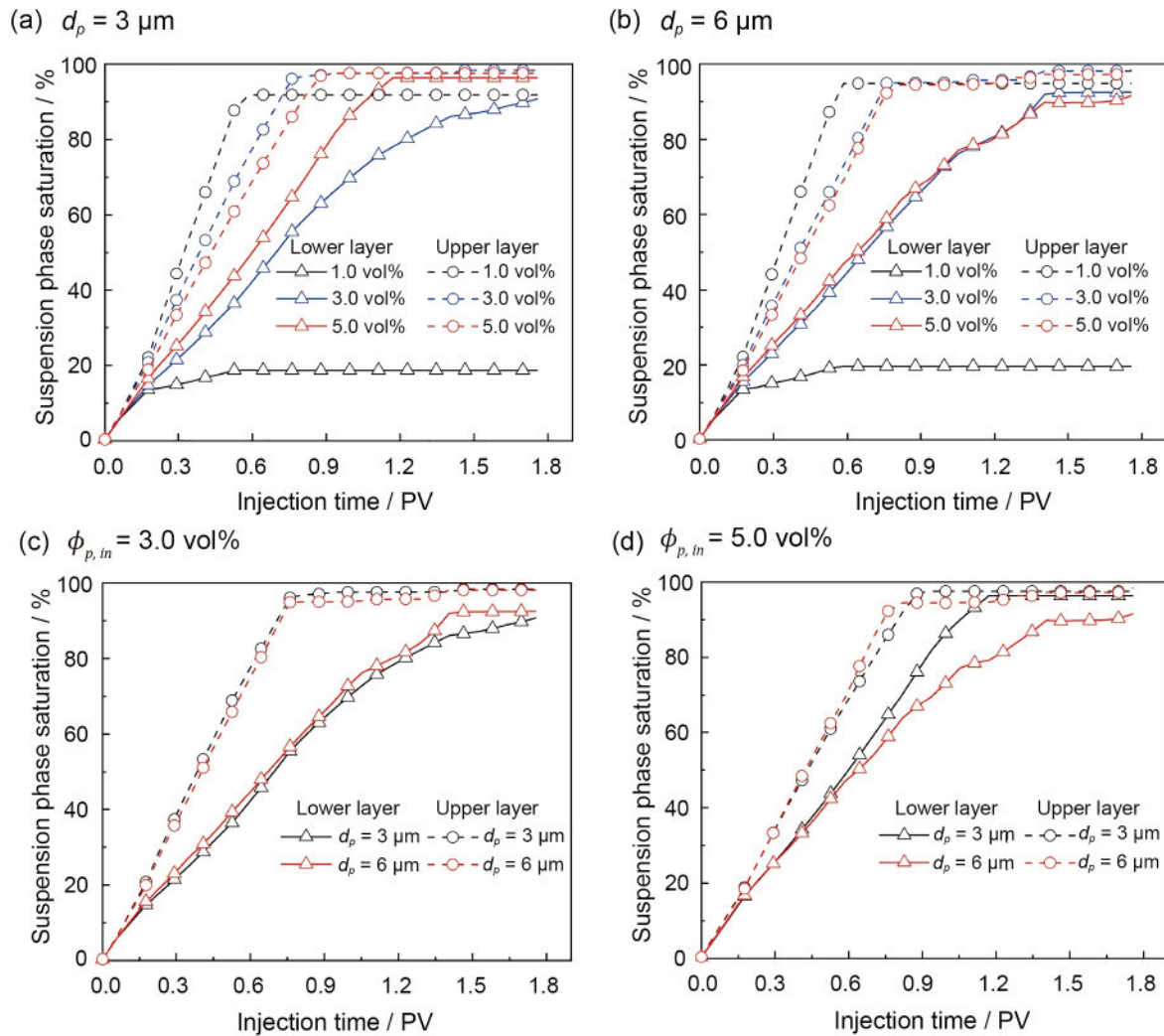


**Figure 6.** Statistics of suspension phase saturation evolution versus injection time. (a, b) Concentration effect under different sizes. (c, d) Size effect under different concentrations.

### 3.3. Results in the Complex Disordered Medium

The complex pore size variations in the disordered medium naturally strengthen particle accumulation, which has promising potential for immiscible displacement control. As shown in Figure 8, the injection of microgel particle suspensions significantly improves displacement efficiency compared to waterflooding (0.0 vol%) under all conditions, with a maximal efficiency increase of 15%. Size and concentration effects on the displacement performance result in efficiency variations within 6%. As discussed in Section 3.2, larger particle sizes and higher injection concentrations promote accumulation. Meanwhile, an intermediate accumulation state is more favorable for displacement enhancement, which results in non-trivial evolution trend in disordered media. At a smaller particle size ( $d_p = 3 \mu\text{m}$ ), the displacement efficiency increases monotonically versus concentration with the rate of change gradually decreasing, indicating improved diversion effects by moderate accumulation. At a larger particle size ( $d_p = 6 \mu\text{m}$ ), the ultimate efficiency is always lower than that at a smaller size, corresponding to limited penetration due to stronger filter-cake effects, which will be further discussed in Figure 10. The non-monotonic fluctuating trend versus concentration reflects the interplay between the favorable viscosity increase and the unfavorable weakening of diversion effect, both driven by intensified accumulation.

As depicted in Figure 9a, sweeping efficiency improvement via diversion effect is the dominant mechanism for enhanced displacement by microgel particle suspensions. The local accumulation effects are responsible for this

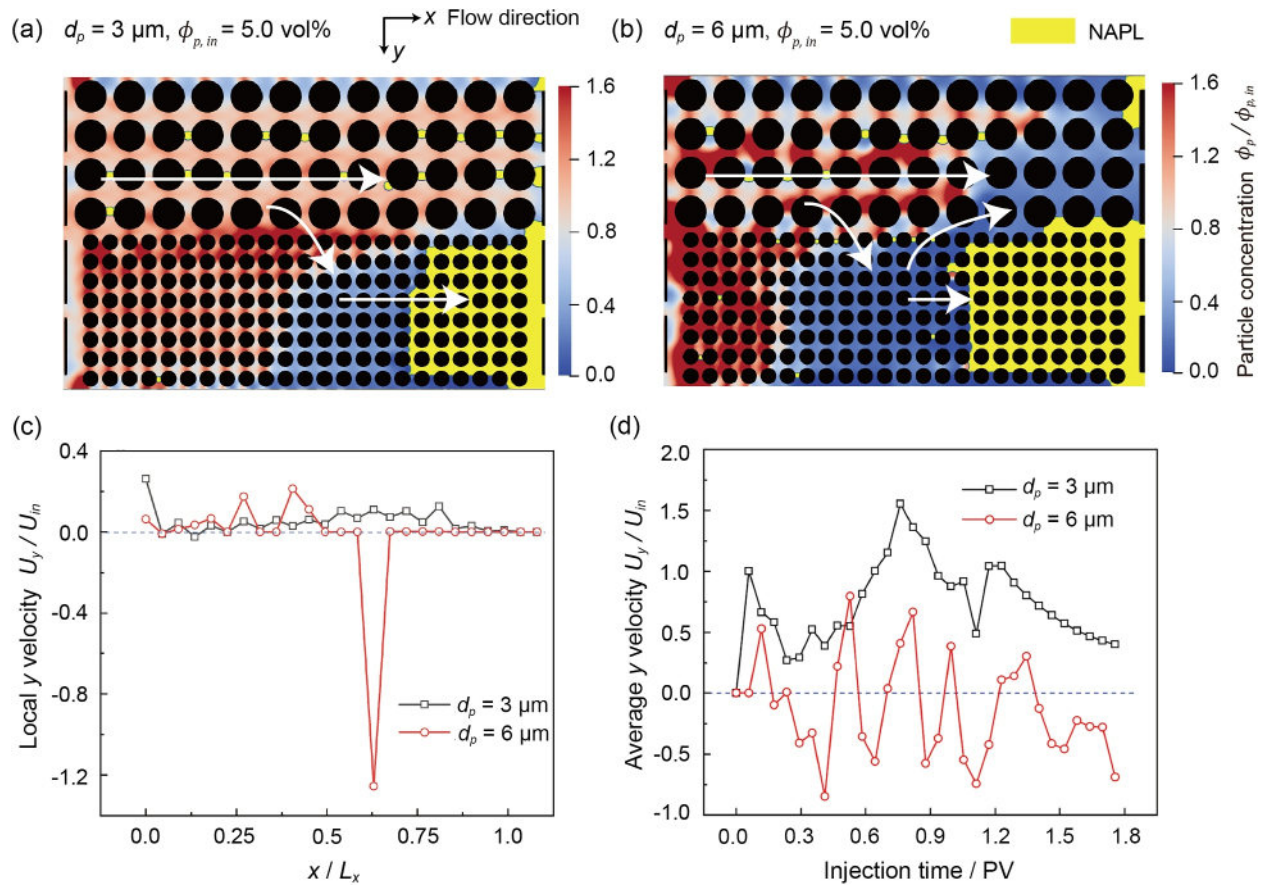


**Figure 7.** Particle accumulation effect on flow patterns during displacement in the dual-permeability model. (a, b) Particle-water-NAPL distribution at different particle sizes when  $\phi_{p,in} = 5.0 \text{ vol}\%$  after 0.9 PV of injection. The white arrows illustrate different lateral flow modes controlled by filter-cake-like distribution. (c) The local lateral flow rates crossing the layer interface with respect to the position along the flow direction after 0.9 PV of injection. The velocity is normalized by the inlet velocity  $U_{in}$ , and  $L_x$  is the length of the porous region ( $L_x = 8 \text{ mm}$ ). (d) Evolution of the total lateral flow rate crossing the layer interface with respect to injection time.

enhancement, as the increased resistance at the accumulation points can divert the invading fluid into other unswept regions (Figures 9b–9d).

To interpret the size dependence of displacement efficiency, particle distributions throughout the disordered medium are compared and analyzed. As shown in Figures 10a and 10b, a stronger upstream accumulation effect with filter-cake-like distribution hinders particle penetration, leading to weaker in-depth diversion effect. As exemplified in Figures 10c and 10d, the moderate accumulation state of particles with a smaller size can divert downstream fluid from the preferential pathway into the unswept region. Instead, particles with a larger size pose negligible impact on the local flow rate allocation. The characteristic speed remains higher in the preferential pathway and less residual NAPL in region 3 (Figure 9) has been removed.

The results presented above offer a new perspective for understanding particle behaviors in porous media, where the concentration-sensitive viscosity of microgel particles serves as the basis for pronounced accumulation and the velocity variations in porous media serve as the triggering factor. The discussed impacts of geometric, flow and particle property conditions on accumulation patterns and displacement performances yield broad implications for subsurface scenarios related to particle transport under multiphase flow conditions. Although the improved numerical model based on a Eulerian–Eulerian description for particulate flow is much more efficient in comparison to previous studies under Eulerian–Lagrangian framework, the descriptions fall within the pore scale and the simulation domain is limited to microfluidic porous media. Regardless, the mechanisms regarding particle accumulation revealed in this work offer a basis for upscaling at larger scales via colloid filtration theory (Mays & Hunt, 2005; Molnar et al., 2015) or pore-network models (H. Yang & Balhoff, 2017). For instance, continuum models for emulsion flow have been developed for capturing the pure viscosity effect (Alvarado &

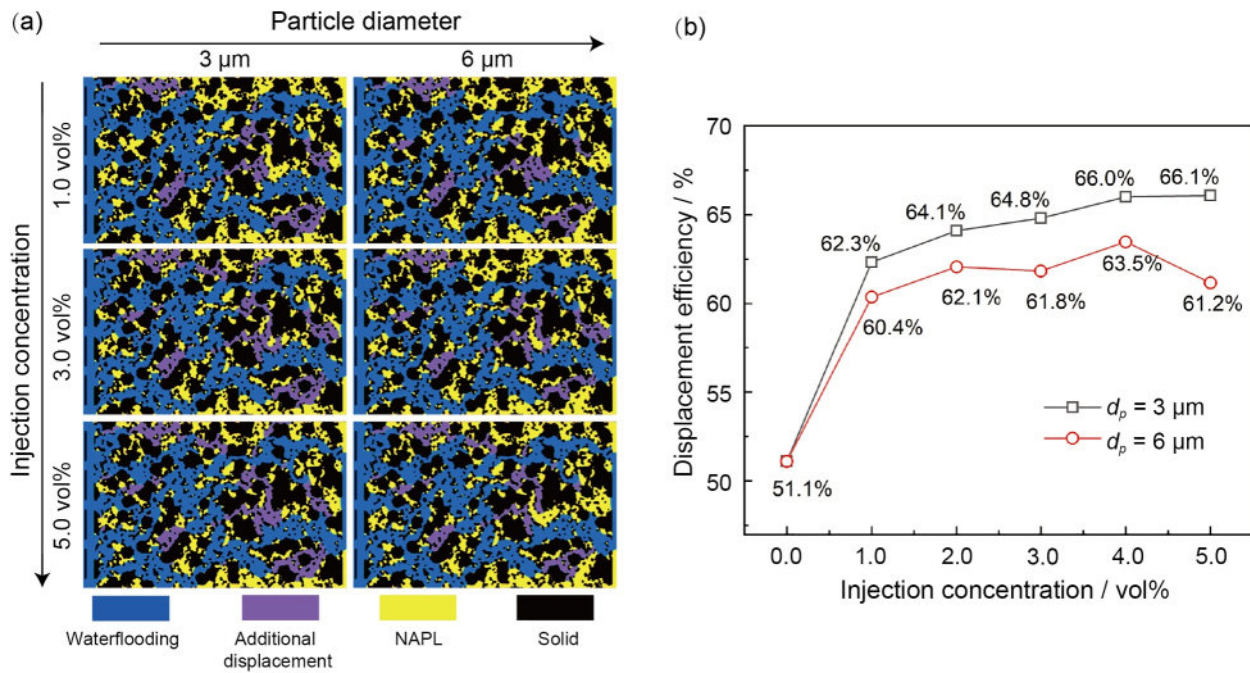


**Figure 8.** Displacement performances in the disordered medium. (a) Phase distribution at the final stage. (b) Statistics of displacement efficiency (suspension phase saturation at the final stage) as a function of injection concentration and particle size.

Marsden, 1979), the capillary Jamin effect (Devereux, 1974), and retention mechanisms including straining and interception (Soo et al., 1986; Soo and Radke, 1984, 1986). The specific upscaling technique for the reported accumulation effects should be addressed in future work by quantifying the accumulation criterion based on the microscopic force competition, and introducing its contribution into macroscopic governing equations.

#### 4. Conclusions

In summary, we systematically investigate non-clogging accumulation effect on microgel particle transport and immiscible displacement in porous media. Triggered by velocity variations in porous media, the lagging of microgel particles can induce strong accumulation owing to the concentration-sensitive viscosity. We utilize a numerical model combining the mixture-rheology two-fluid model for particle transport and the color-gradient

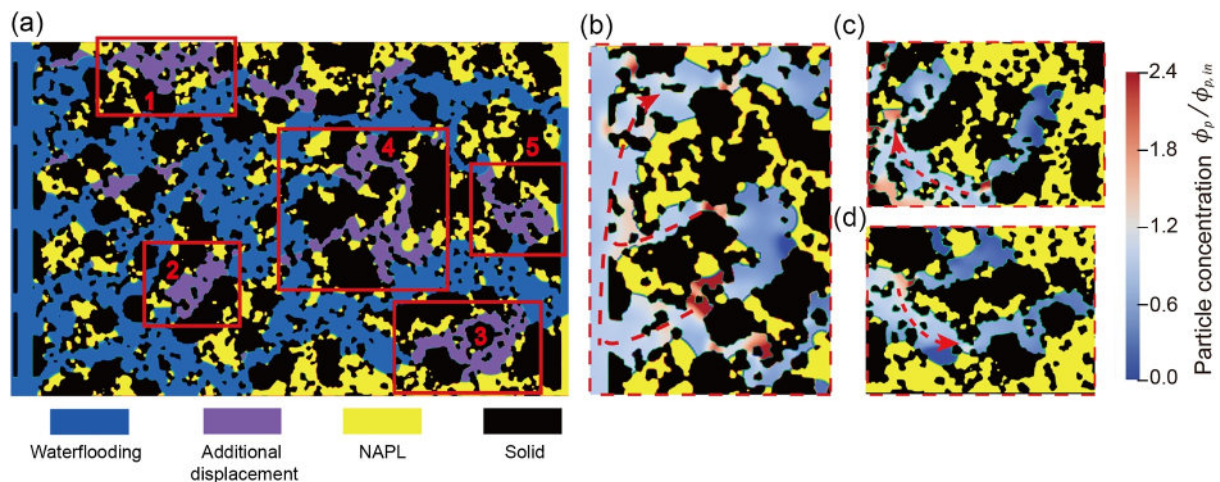


**Figure 9.** The relationship between (a) sweeping efficiency improvement and (b–d) local accumulation and diversion effect ( $d_p = 3 \mu\text{m}$ ,  $\phi_{p,in} = 3.0 \text{ vol}\%$ ). The local views in (b–d) correspond to the invasion into region 1–3 in (a), respectively.

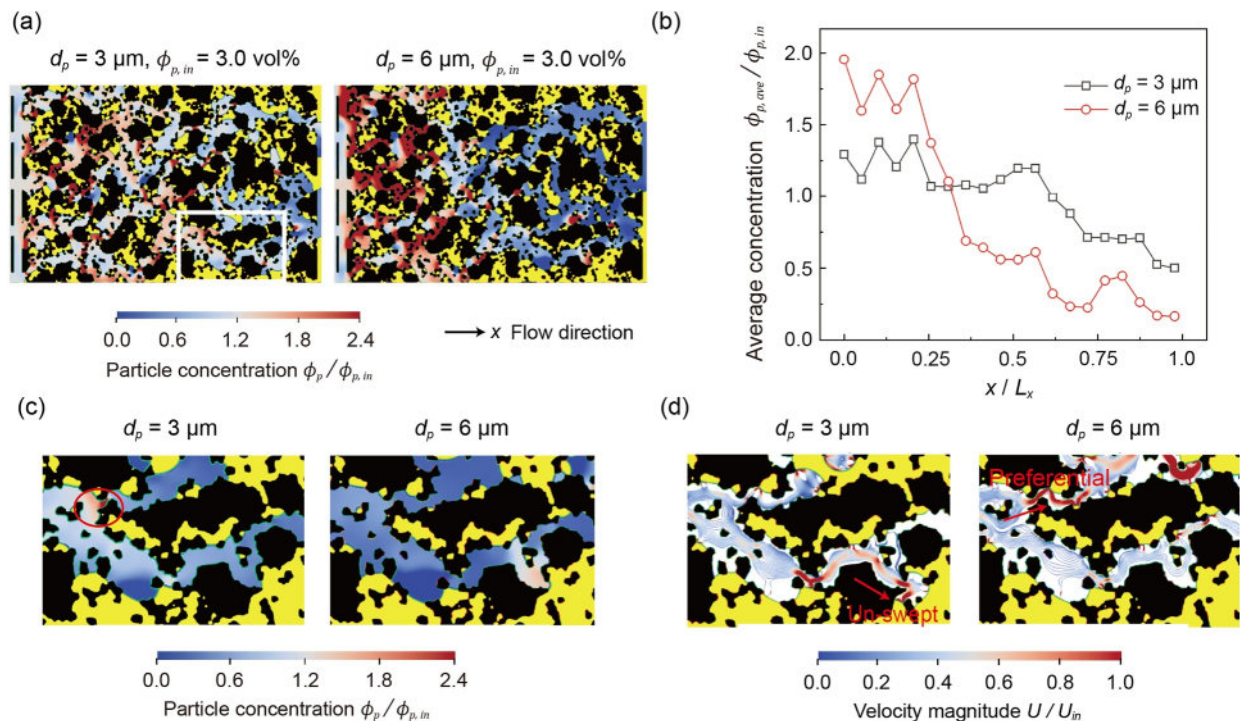


**Figure 10.** Size effect on particle accumulation and displacement patterns in the disordered medium. (a) Global distribution at the final stage (1.8 PV) for different particle sizes when  $\phi_{p,in} = 3.0 \text{ vol}\%$ . (b) Quantification of the local average particle concentration along the flow direction ( $L_x = 8 \text{ mm}$ ). (c, d) Examples of (c) local concentration distribution and (d) corresponding velocity distribution at different sizes after 1.2 PV of injection. The field of view is denoted by the white box in (a) and the alternation of flow direction in this region determines displacement in region 3 of Figure 9.

lattice Boltzmann method for immiscible displacement to capture accumulation behaviors under multiphase flow conditions, which has been successfully applied to reproduce the anomalous accumulation phenomena reported in previous experiments. Building on a series of investigations in the dual-permeability porous structure, we unravel the force competition behind accumulation patterns and clarify the influencing factors on accumulation intensity. Particle accumulation can be strengthened by an increased particle size, elevated injection concentration, and additional capillary resistance introduced by immiscible interfaces. Accumulation patterns are also influenced by both structural and flow conditions, where lower local permeability and lower characteristic velocity promote preferential accumulation. The formation and distribution of filter-cake-like structures reflect intensified local accumulation, which diverts fluid into other regions by lateral flow and promotes the displacement of residual NAPL. Investigations in the complex disordered medium demonstrates the generality of our analysis, where sweeping efficiency can be dramatically improved via local accumulation and self-adaptive diversion. An intermediate accumulation state, commonly characterized by a smaller particle size at high injection concentration, most benefits displacement control in porous media.

Our results provide a new paradigm for predicting and controlling particle transport and multiphase flow in subsurface environments. Moving forward, more factors require consideration for engineering applications, such as determining optimal size and concentration conditions, quantifying structural heterogeneity effects, and incorporating other particle behaviors including deformation.

### Data Availability Statement

The original data sets for presented cases are available at Mendeley Data (Lu, 2025).

### References

Adamczyk, Z., & Weroński, P. (1999). Application of the DLVO theory for particle deposition problems. *Advances in Colloid and Interface Science*, 83(1), 137–226. [https://doi.org/10.1016/S0001-8686\(99\)00009-3](https://doi.org/10.1016/S0001-8686(99)00009-3)

### Acknowledgments

This work is financially supported by the NSF grant of China (No. U24B6003, 12432013, 12272207) and the National Key Research and Development Program of China (No. 2019YFA0708704).

- Akai, T., Bijeljic, B., & Blunt, M. J. (2018). Wetting boundary condition for the color-gradient lattice Boltzmann method: Validation with analytical and experimental data. *Advances in Water Resources*, *116*, 56–66. <https://doi.org/10.1016/j.advwatres.2018.03.014>
- Alvarado, D. A., & Marsden, S. S., Jr. (1979). Flow of oil-in-water emulsions through tubes and porous media. *Society of Petroleum Engineers Journal*, *19*(6), 369–377. <https://doi.org/10.2118/5859-pa>
- Bai, B., Liu, Y., Coste, J.-P., & Li, L. (2007). Preformed particle gel for conformance control: Transport mechanism through porous media. *SPE Reservoir Evaluation and Engineering*, *10*(2), 176–184. <https://doi.org/10.2118/89468-pa>
- Barns, S., Balanant, M. A., Sauret, E., Flower, R., Saha, S., & Gu, Y. (2017). Investigation of red blood cell mechanical properties using AFM indentation and coarse-grained particle method. *BioMedical Engineering Online*, *16*(1), 140. <https://doi.org/10.1186/s12938-017-0429-5>
- Batchelor, G. K. (1977). The effect of Brownian motion on the bulk stress in a suspension of spherical particles. *Journal of Fluid Mechanics*, *83*(1), 97–117. <https://doi.org/10.1017/S0022112077001062>
- Bizmark, N., Schneider, J., Priestley, R. D., & Datta, S. S. (2020). Multiscale dynamics of colloidal deposition and erosion in porous media. *Science Advances*, *6*(46), eabc2530. <https://doi.org/10.1126/sciadv.abc2530>
- Brackbill, J. U., Kothe, D. B., & Zemach, C. (1992). A continuum method for modeling surface tension. *Journal of Computational Physics*, *100*(2), 335–354. [https://doi.org/10.1016/0021-9991\(92\)90240-Y](https://doi.org/10.1016/0021-9991(92)90240-Y)
- Chen, S., & Doolen, G. D. (1998). Lattice Boltzmann method for fluid flows. *Annual Review of Fluid Mechanics*, *30*(1), 329–364. <https://doi.org/10.1146/annurev.fluid.30.1.329>
- Chien, S. (1987). Red cell deformability and its relevance to blood flow. *Annual Review of Physiology*, *49*(1), 177–192. <https://doi.org/10.1146/annurev.ph.49.030187.001141>
- Chu, K. W., Kuang, S. B., Yu, A. B., & Zhou, Z. Y. (2010). Discrete particle simulation of particle–fluid flow: Model formulations and their applicability. *Journal of Fluid Mechanics*, *661*, 482–510. <https://doi.org/10.1017/S002211201000306X>
- Devereux, O. F. (1974). Emulsion flow in porous solids: I. A flow model. *The Chemical Engineering Journal*, *7*(2), 121–128. [https://doi.org/10.1016/0300-9467\(74\)85005-7](https://doi.org/10.1016/0300-9467(74)85005-7)
- Ding, J., & Gidaspow, D. (1990). A bubbling fluidization model using kinetic theory of granular flow. *AIChE Journal*, *36*(4), 523–538. <https://doi.org/10.1002/aic.690360404>
- Dressaire, E., & Sauret, A. (2017). Clogging of microfluidic systems. *Soft Matter*, *13*(1), 37–48. <https://doi.org/10.1039/C6SM01879C>
- Drew, D. A. (1983). Mathematical modeling of two-phase flow. *Annual Review of Fluid Mechanics*, *15*(1), 261–291. <https://doi.org/10.1146/annurev.fl.15.010183.001401>
- Du, Y., Xu, K., Mejia, L., & Balhoff, M. (2021). A coreflood-on-a-chip study of viscoelasticity's effect on reducing residual saturation in porous media. *Water Resources Research*, *57*(8), e2021WR029688. <https://doi.org/10.1029/2021WR029688>
- Dye, A. L., McClure, J. E., Adalsteinsson, D., & Miller, C. T. (2016). An adaptive lattice Boltzmann scheme for modeling two-fluid-phase flow in porous medium systems. *Water Resources Research*, *52*(4), 2601–2617. <https://doi.org/10.1002/2015WR018279>
- Elrahmani, A., Al-Raoush, R. I., & Seers, T. D. (2023). Clogging and permeability reduction dynamics in porous media: A numerical simulation study. *Powder Technology*, *427*, 118736. <https://doi.org/10.1016/j.powtec.2023.118736>
- Endo Kokubun, M. A., Radu, F. A., Keilegavlen, E., Kumar, K., & Spildo, K. (2019). Transport of polymer particles in oil–water flow in porous media: Enhancing oil recovery. *Transport in Porous Media*, *126*(2), 501–519. <https://doi.org/10.1007/s11242-018-1175-2>
- Gerber, G., Rodts, S., Aimeidieu, P., Faure, P., & Coussot, P. (2018). Particle-size-exclusion clogging regimes in porous media. *Physical Review Letters*, *120*(14), 148001. <https://doi.org/10.1103/PhysRevLett.120.148001>
- Gidaspow, D. (1994). *Multiphase flow and fluidization: Continuum and kinetic theory descriptions*. Academic Press.
- Grad, H. (1949). On the kinetic theory of rarefied gases. *Communications on Pure and Applied Mathematics*, *2*(4), 331–407. <https://doi.org/10.1002/cpa.3160020403>
- Guazzelli, É., & Pouliquen, O. (2018). Rheology of dense granular suspensions. *Journal of Fluid Mechanics*, *852*, P1. <https://doi.org/10.1017/jfm.2018.548>
- Guo, Z., Zheng, C., & Shi, B. (2002). Discrete lattice effects on the forcing term in the lattice Boltzmann method. *Physical Review E*, *65*(4), 046308. <https://doi.org/10.1103/PhysRevE.65.046308>
- He, G., Ming, P., Zhao, Z., Abudula, A., & Xiao, Y. (2007). A two-fluid model for two-phase flow in PEMFCs. *Journal of Power Sources*, *163*(2), 864–873. <https://doi.org/10.1016/j.jpowsour.2006.09.059>
- Katzourakis, V. E., & Chrysikopoulos, C. V. (2021). Modeling the transport of aggregating nanoparticles in porous media. *Water Resources Research*, *57*(1), e2020WR027946. <https://doi.org/10.1029/2020WR027946>
- Koch, D. L., & Hill, R. J. (2001). Inertial effects in suspension and porous-media flows. *Annual Review of Fluid Mechanics*, *33*(1), 619–647. <https://doi.org/10.1146/annurev.fluid.33.1.619>
- Ladd, A. J. C. (1994). Numerical simulations of particulate suspensions via a discretized Boltzmann equation. Part 1. Theoretical foundation. *Journal of Fluid Mechanics*, *271*, 285–309. <https://doi.org/10.1017/S0022112094001771>
- Lallemand, P., & Luo, L.-S. (2000). Theory of the lattice Boltzmann method: Dispersion, dissipation, isotropy, Galilean invariance, and stability. *Physical Review E*, *61*(6), 6546–6562. <https://doi.org/10.1103/PhysRevE.61.6546>
- Larson, R. G., & Desai, P. S. (2015). Modeling the rheology of polymer melts and solutions. *Annual Review of Fluid Mechanics*, *47*(1), 47–65. <https://doi.org/10.1146/annurev-fluid-010814-014612>
- Latva-Kokko, M., & Rothman, D. H. (2005). Diffusion properties of gradient-based lattice Boltzmann models of immiscible fluids. *Physical Review E*, *71*(5), 056702. <https://doi.org/10.1103/PhysRevE.71.056702>
- Leclaire, S., Pellerin, N., Reggio, M., & Trépanier, J. Y. (2014). Unsteady immiscible multiphase flow validation of a multiple-relaxation-time lattice Boltzmann method. *Journal of Physics A: Mathematical and Theoretical*, *47*(10), 105501. <https://doi.org/10.1088/1751-8113/47/10/105501>
- Leclaire, S., Reggio, M., & Trépanier, J.-Y. (2011). Isotropic color gradient for simulating very high-density ratios with a two-phase flow lattice Boltzmann model. *Computers & Fluids*, *48*(1), 98–112. <https://doi.org/10.1016/j.compfluid.2011.04.001>
- Leclaire, S., Reggio, M., & Trépanier, J.-Y. (2013). Progress and investigation on lattice Boltzmann modeling of multiple immiscible fluids or components with variable density and viscosity ratios. *Journal of Computational Physics*, *246*, 318–342. <https://doi.org/10.1016/j.jcp.2013.03.039>
- Lei, W., Li, Q., Yang, H.-E., Wu, T.-J., Wei, J., & Wang, M. (2022). Preferential flow control in heterogeneous porous media by concentration-manipulated rheology of microgel particle suspension. *Journal of Petroleum Science and Engineering*, *212*, 110275. <https://doi.org/10.1016/j.petrol.2022.110275>
- Lei, W., Lu, X., & Wang, M. (2023). Multiphase displacement manipulated by micro/nanoparticle suspensions in porous media via microfluidic experiments: From interface science to multiphase flow patterns. *Advances in Colloid and Interface Science*, *311*, 102826. <https://doi.org/10.1016/j.cis.2022.102826>

- Lei, W., Xie, C., Wu, T., Wu, X., & Wang, M. (2019). Transport mechanism of deformable micro-gel particle through micropores with mechanical properties characterized by AFM. *Scientific Reports*, 9(1), 1453. <https://doi.org/10.1038/s41598-018-37270-7>
- Li, Q., Yang, G., Huang, Y., Lu, X., Min, J., & Wang, M. (2024). Lattice Boltzmann method for particulate multiphase flow system. *International Journal of Mechanical Sciences*, 273, 109217. <https://doi.org/10.1016/j.ijmecsci.2024.109217>
- Lin, D., Hu, L., Bradford, S. A., Zhang, X., & Lo, I. M. C. (2021). Simulation of colloid transport and retention using a pore-network model with roughness and chemical heterogeneity on pore surfaces. *Water Resources Research*, 57(2), e2020WR028571. <https://doi.org/10.1029/2020WR028571>
- Liu, H., Ju, Y., Wang, N., Xi, G., & Zhang, Y. (2015). Lattice Boltzmann modeling of contact angle and its hysteresis in two-phase flow with large viscosity difference. *Physical Review E*, 92(3), 033306. <https://doi.org/10.1103/PhysRevE.92.033306>
- Lou, Q., Guo, Z., & Shi, B. (2013). Evaluation of outflow boundary conditions for two-phase lattice Boltzmann equation. *Physical Review E*, 87(6), 063301. <https://doi.org/10.1103/PhysRevE.87.063301>
- Lu, X. (2025). Pore-scale study of non-clogging accumulation effects on microgel particle transport and multiphase displacements in porous media [Dataset]. *Mendeley data*. <https://doi.org/10.17632/w95tzhd6v.1>
- Lu, X., & Wang, M. (2023). High-performance nanogel-in-oils as emulsion evolution controller for displacement enhancement in porous media. *ACS Applied Materials & Interfaces*, 15(42), 49554–49566. <https://doi.org/10.1021/acsami.3c05576>
- Massoudi, M., Kim, J., & Antaki, J. F. (2012). Modeling and numerical simulation of blood flow using the theory of interacting continua. *International Journal of Non-Linear Mechanics*, 47(5), 506–520. <https://doi.org/10.1016/j.ijnonlinmec.2011.09.025>
- Mays, D. C., & Hunt, J. R. (2005). Hydrodynamic aspects of particle clogging in porous media. *Environmental Science & Technology*, 39(2), 577–584. <https://doi.org/10.1021/es049367k>
- Molnar, I. L., Johnson, W. P., Gerhard, J. I., Willson, C. S., & O'Carroll, D. M. (2015). Predicting colloid transport through saturated porous media: A critical review. *Water Resources Research*, 51(9), 6804–6845. <https://doi.org/10.1002/2015WR017318>
- O'Carroll, D., Sleep, B., Krol, M., Boparai, H., & Kocur, C. (2013). Nanoscale zero valent iron and bimetallic particles for contaminated site remediation. *Advances in Water Resources*, 51, 104–122. <https://doi.org/10.1016/j.advwatres.2012.02.005>
- Pak, T., Luz, L., Tosco, T., Costa, G. S. R., Rosa, P. R. R., & Archilha, N. L. (2020). Pore-scale investigation of the use of reactive nanoparticles for in situ remediation of contaminated groundwater source. *Proceedings of the National Academy of Sciences of the United States of America*, 117(24), 13366–13373. <https://doi.org/10.1073/pnas.1918683117>
- Qin, F., Fei, L., Zhao, J., Kang, Q., Derome, D., & Carmeliet, J. (2023). Lattice Boltzmann modelling of colloidal suspensions drying in porous media accounting for local nanoparticle effects. *Journal of Fluid Mechanics*, 963, A26. <https://doi.org/10.1017/jfm.2023.344>
- Riaud, A., Zhao, S., Wang, K., Cheng, Y., & Luo, G. (2014). Lattice-Boltzmann method for the simulation of multiphase mass transfer and reaction of dilute species. *Physical Review E*, 89(5), 053308. <https://doi.org/10.1103/PhysRevE.89.053308>
- Roy, S. B., & Dzombak, D. A. (1997). Chemical factors influencing colloid-facilitated transport of contaminants in porous media. *Environmental Science & Technology*, 31(3), 656–664. <https://doi.org/10.1021/es9600643>
- Semiao, V., & Silva, G. (2012). First- and second-order forcing expansions in a lattice Boltzmann method reproducing isothermal hydrodynamics in artificial compressibility form. *Journal of Fluid Mechanics*, 698, 282–303. <https://doi.org/10.1017/jfm.2012.83>
- Shuai, W., Zhenhua, H., Huilin, L., Goudong, L., Jiaying, W., & Pengfei, X. (2012). A bubbling fluidization model using kinetic theory of rough spheres. *AIChE Journal*, 58(2), 440–455. <https://doi.org/10.1002/aic.12590>
- Sim, Y., & Chrysikopoulos, C. V. (2000). Virus transport in unsaturated porous media. *Water Resources Research*, 36(1), 173–179. <https://doi.org/10.1029/1999WR900302>
- Soo, H., & Radke, C. J. (1984). Flow mechanism of dilute, stable emulsions in porous media. *Industrial & Engineering Chemistry Fundamentals*, 23(3), 342–347. <https://doi.org/10.1021/i100015a014>
- Soo, H., & Radke, C. J. (1986). A filtration model for the flow of dilute, stable emulsions in porous media—I. Theory. *Chemical Engineering Science*, 41(2), 263–272. [https://doi.org/10.1016/0009-2509\(86\)87007-5](https://doi.org/10.1016/0009-2509(86)87007-5)
- Soo, H., Williams, M. C., & Radke, C. J. (1986). A filtration model for the flow of dilute, stable emulsions in porous media—II. Parameter evaluation and estimation. *Chemical Engineering Science*, 41(2), 273–281. [https://doi.org/10.1016/0009-2509\(86\)87008-7](https://doi.org/10.1016/0009-2509(86)87008-7)
- Spildo, K., Skauge, A., Aarra, M. G., & Tveheyo, M. T. (2009). A new polymer application for north sea reservoirs. *SPE Reservoir Evaluation and Engineering*, 12(3), 427–432. <https://doi.org/10.2118/113460-pa>
- Su, J., Chai, G., Wang, L., Cao, W., Gu, Z., Chen, C., & Xu, X. Y. (2019). Pore-scale direct numerical simulation of particle transport in porous media. *Chemical Engineering Science*, 199, 613–627. <https://doi.org/10.1016/j.ces.2019.01.033>
- Trofa, M., D'Avino, G., & Maffettone, P. L. (2021). Numerical simulation of clogging in a microchannel with planar contraction. *Physics of Fluids*, 33(8). <https://doi.org/10.1063/5.0061353>
- van der Hoef, M. A., Annaland, M. V. S., Deen, N. G., & Kuipers, J. A. M. (2008). Numerical simulation of dense gas-solid fluidized beds: A multiscale modeling strategy. *Annual Review of Fluid Mechanics*, 40(1), 47–70. <https://doi.org/10.1146/annurev.fluid.40.111406.102130>
- Wang, H., Lin, M., Chen, D., Dong, Z., Yang, Z., & Zhang, J. (2018). Research on the rheological properties of cross-linked polymer microspheres with different microstructures. *Powder Technology*, 331, 310–321. <https://doi.org/10.1016/j.powtec.2018.03.045>
- Wang, M., Wang, J., Pan, N., & Chen, S. (2007). Mesoscopic predictions of the effective thermal conductivity for microscale random porous media. *Physical Review E*, 75(3), 036702. <https://doi.org/10.1103/PhysRevE.75.036702>
- Wang, T., & Wang, J. (2005). Two-fluid model based on the lattice Boltzmann equation. *Physical Review E*, 71(4), 045301. <https://doi.org/10.1103/PhysRevE.71.045301>
- Wen, C. Y., & Yu, Y. H. (1966). Mechanics of fluidization. In *Paper presented at chemical engineering progress symposium series, American Institute of Chemical Engineers*.
- Wood, B. D. (2007). Inertial effects in dispersion in porous media. *Water Resources Research*, 43(12), W12S16. <https://doi.org/10.1029/2006WR005790>
- Wu, W.-T., Yang, F., Antaki, J. F., Aubry, N., & Massoudi, M. (2015). Study of blood flow in several benchmark micro-channels using a two-fluid approach. *International Journal of Engineering Science*, 95, 49–59. <https://doi.org/10.1016/j.ijengsci.2015.06.004>
- Xie, C., Lei, W., Balhoff, M. T., Wang, M., & Chen, S. (2021). Self-adaptive preferential flow control using displacing fluid with dispersed polymers in heterogeneous porous media. *Journal of Fluid Mechanics*, 906, A10. <https://doi.org/10.1017/jfm.2020.763>
- Xie, C., Zhang, J., Bertola, V., & Wang, M. (2016). Lattice Boltzmann modeling for multiphase viscoplastic fluid flow. *Journal of Non-Newtonian Fluid Mechanics*, 234, 118–128. <https://doi.org/10.1016/j.jnnfm.2016.05.003>
- Xu, K., Zhu, P., Huh, C., & Balhoff, M. T. (2015). Microfluidic investigation of nanoparticles' role in mobilizing trapped oil droplets in porous media. *Langmuir*, 31(51), 13673–13679. <https://doi.org/10.1021/acs.langmuir.5b03733>
- Yang, G., Chen, Y., Chen, S., & Wang, M. (2023). Implementation of a direct-addressing based lattice Boltzmann GPU solver for multiphase flow in porous media. *Computer Physics Communications*, 291, 108828. <https://doi.org/10.1016/j.cpc.2023.108828>

- Yang, H., & Balhoff, M. T. (2017). Pore-network modeling of particle retention in porous media. *AIChE Journal*, *63*(7), 3118–3131. <https://doi.org/10.1002/aic.15593>
- Yin, Y., Cui, Y., & Jing, L. (2024). Clogging and unclogging of fine particles in porous media: Micromechanical insights from an analog pore system. *Water Resources Research*, *60*(1), e2023WR034628. <https://doi.org/10.1029/2023WR034628>
- Yu, Y., Elliott, M., Chowdhury, I., & Flury, M. (2021). Transport mechanisms of motile and nonmotile phytophthora cactorum zoospores in unsaturated porous media. *Water Resources Research*, *57*(2), e2020WR028249. <https://doi.org/10.1029/2020WR028249>
- Yu, Z., & Fan, L.-S. (2010). Multirelaxation-time interaction-potential-based lattice Boltzmann model for two-phase flow. *Physical Review E*, *82*(4), 046708. <https://doi.org/10.1103/physreve.82.046708>
- Zhang, H., Ramakrishnan, T. S., Nikolov, A., & Wasan, D. (2016). Enhanced oil recovery driven by nanofilm structural disjoining pressure: Flooding experiments and microvisualization. *Energy & Fuels*, *30*(4), 2771–2779. <https://doi.org/10.1021/acs.energyfuels.6b00035>
- Zhou, K., Hou, J., Sun, Q., Guo, L., Bing, S., Du, Q., & Yao, C. (2017). An efficient LBM-DEM simulation method for suspensions of deformable preformed particle gels. *Chemical Engineering Science*, *167*, 288–296. <https://doi.org/10.1016/j.ces.2017.04.026>
- Zhu, H. P., Zhou, Z. Y., Yang, R. Y., & Yu, A. B. (2007). Discrete particle simulation of particulate systems: Theoretical developments. *Chemical Engineering Science*, *62*(13), 3378–3396. <https://doi.org/10.1016/j.ces.2006.12.089>
- Zou, Q., & He, X. (1997). On pressure and velocity boundary conditions for the lattice Boltzmann BGK model. *Physics of Fluids*, *9*(6), 1591–1598. <https://doi.org/10.1063/1.869307>